



Ultra-strong and stiff randomly-oriented discontinuous composites: Closing the gap to quasi-isotropic continuous-fibre laminates

M. Alves^a, D. Carlstedt^b, F. Ohlsson^c, L.E. Asp^b, S. Pimenta^{a,*}

^a *meComposites, Department of Mechanical Engineering, Imperial College London, South Kensington Campus, London SW7 2AZ, UK*

^b *Department of Industrial and Materials Science, Chalmers University of Technology, SE-41296 Gothenburg, Sweden*

^c *Oxeon AB, Borås, Sweden*

ARTICLE INFO

Keywords:

- A. Discontinuous reinforcement
- B. Stress transfer
- C. Analytical modelling
- D. Mechanical testing

ABSTRACT

Conventional randomly-oriented Tow Based Discontinuous Composites (TBDCs) are materials which combine good mechanical properties, lightweight and high manufacturability, and are therefore interesting for high-volume transport industries. This paper proposes, designs and successfully demonstrates a pathway to produce TBDCs with outstanding stiffness and tensile strength, by using ultra-thin tapes of (ultra-) high modulus carbon-fibres. Numerical models are used to explore the design space of discontinuous composite materials, in order to identify the optimal microstructural design to maximise stiffness and strength. Selected microstructures are manufactured and tested under tension; the experimental results show good agreement with the numerical predictions, and demonstrate a significant increase in the tensile strength and Young's modulus of TBDCs by reducing the tow thickness and increasing the modulus of the fibres. Strength and stiffness increases of over 100% compared with the commercially available TBDC systems are achieved, resulting in mechanical properties that match the strength and overcome the stiffness of aerospace-graded continuous-fibre laminates.

1. Introduction

Tow Based Discontinuous Composites (TBDCs) are an up and coming class of high-performance composite materials that consist of long chopped carbon fibre tows randomly distributed in a polymeric matrix. The random and discontinuous nature of the material makes it more manufacturable than conventional continuous-fibre composites; in addition, high fibre volume fractions (up to 60%) are achievable with this type of microstructure, which leads to high mechanical properties [1–7]. Some examples of current commercial applications of TBDCs include window frames of the 787 Dreamliner [8] and helicopter tail-boom frames [9].

Commercially available TBDCs are based either on chopped prepreg [10] or Sheet Moulding Compounds (SMC) [11]; in these commercially available systems, the in-plane randomness of the tows is achieved through proprietary processes. Lab-based TBDCs are usually manufactured by chopping prepreg [3,5,12]; in these lab-based systems, the in-plane randomness of the tows was achieved through a variety of processes, eg. by manually placing each individual tow in a location and orientation previously defined by a numerical random number generator [5], by a wet-type paper making process where the tows are randomly dispersed in water [12], or by scattering all tows at once until

achieving a visually satisfactory degree of randomisation [3].

Compression moulded TBDC specimens have shown stiffness values comparable to those of quasi-isotropic continuous-fibre laminates [2,3], hence making them a good alternative to continuous fibre composites for stiffness-driven designs. Moreover, due to the material architecture, with stiff inclusions embedded in a soft matrix, high damage tolerance has been achieved [13,14].

However, the discontinuous architecture of TBDCs leads to stress concentrations near the tow-ends, which generate damage at the interface between tows, potentially leading to failure due to tow debonding and pull-out. For this reason, the strength values of commercially available TBDCs are significantly (between 30 and 60%) lower than those of quasi-isotropic continuous-fibre laminates [2].

It has been experimentally shown that the thickness of the tows has a significant effect on the mechanical properties of TBDCs [4,5,15]. Wan et al. [4] found that manufacturing TBDCs with thin tows (of approximately 50 μm) resulted in higher ultimate strength values (500 MPa), closer to those of continuous fibre composites. Li et al. [5] manufactured TBDC specimens using two different tow thicknesses (but similar specimen thickness), and found that the specimens with thicker tows led to lower mechanical properties, both in terms of modulus and strength. The latter was attributed to the earlier onset of tow pull-out

* Corresponding author.

E-mail address: soraia.pimenta@imperial.ac.uk (S. Pimenta).

<https://doi.org/10.1016/j.compositesa.2020.105826>

Received 21 November 2019; Received in revised form 5 February 2020; Accepted 8 February 2020

Available online 17 February 2020

1359-835X/ © 2020 Elsevier Ltd. All rights reserved.

that occurs with thick tow configurations, and to the higher variability of the microstructure (as a result of the lower average number of thick tows across the thickness of the specimens), increasing the probability of the occurrence of weak spots in the material.

The use of thin-ply has been shown to significantly increase the mechanical properties of continuous-fibre composite laminates as well. In earlier work by Dvorak and Laws [16], and later by Camanho et al. [17] and Arteiro et al. [18], experimental observations and numerical predictions have shown that the in situ transverse tensile and shear strength increase with the reduction in ply thickness. Moreover, experimental studies by Sihm et al. [19] and Amacher et al. [20] have demonstrated that the stress for the onset of damage and the ultimate tensile strength of quasi-isotropic laminates increase with reduced ply thickness.

Li and Pimenta [21] have predicted the effect of tow thickness on the strength of TBDCs using analytical models specifically developed for these materials. These models were based on (i) equivalent laminates (in which each lamina is an unidirectional discontinuous ply with the same tow geometry as in the actual TBDC [5]) and (ii) shear-lag considering the non-linear shear response of the matrix up to failure [13]. It was shown that it is fundamental to account for the finite fracture toughness of the matrix (or fibre-matrix interface) in the shear-lag formulation [13] in order to correctly predict the effect of tow thickness on the strength of TBDCs.

Other models to predict tensile response of TBDCs have also been presented in the literature [15,22–28]; these models focus either on unidirectional [15,27] or randomly-oriented [22–26,28] composites using either analytical (and therefore efficient) or FE based (and therefore less efficient) formulations. However, some of these models [23,24,26] neglect the effect of delamination between the tows and are therefore unable to capture the effect of the absolute value of the tow thickness on the mechanical response of the material; others [15,27], have focused only on the effect of the tow aspect-ratio rather than on the effect of the absolute value of thickness.

The effect of the specimen thickness on the strength of TBDCs has also been reported in the literature [3,28]. It was shown that the strength decreases with the reduction of the specimen thickness; a strength knock-down of 50% was reported due to a specimen thickness reduction from 3.73 mm down to 0.82 mm. This effect was justified [3,28] by the smaller average number of tows through-the-thickness of the thinner specimen, which increases the variability of properties from one point of the specimen to another, and therefore increases the probability of very weak spots (e.g. with preferentially transverse tows)

that can trigger premature failure.

So far, only TBDC material systems with tow thicknesses ranging from 50 to 200 μm , standard- or intermediate-modulus fibres (below 300 GPa), and plate thickness above 1.5 mm have been tested and reported in the literature [4,10,11,29–31]. The reported tensile-strength values of these TBDC systems range from 250 to 500 MPa [4,10,11,29–31], which are still below the tensile strength of typical continuous-fibre QI laminates (600–900 MPa); moreover, typical tensile moduli of these materials are in the range of 30–50 GPa [4,10,11,29–31], which barely competes with Aluminium in terms of specific stiffness. This leaves room in the design space of the material's microstructure to investigate whether it is possible to achieve higher mechanical properties with this type of architectures. In this work, TBDCs manufactured with ultra-thin (20 μm) and high modulus carbon fibres tows (425–750 GPa) are explored, with the objective to maximise the material's mechanical properties (especially its ultimate tensile strength) and assess its suitability for thinner structures.

In Section 2, physically based numerical models, developed for TBDCs, are used to explore the material's design space and guide the microstructural design. Section 3 details the manufacturing and testing procedures of TBDC plates with different microstructural configurations selected; experimental studies are performed to independently assess how the materials' mechanical properties are affected by the thickness and stiffness of the carbon-fibre tows. The experimental results are analysed and discussed in Sections 4 and 5, and the main conclusions are drawn in Section 6.

2. Material design

2.1. Failure criteria for discontinuous composites

The longitudinal tensile strength and failure mechanisms of discontinuous composites depend on (i) the mechanical properties of the constituents (i.e. fibres and matrix), (ii) the geometry of the reinforcing units (rectangular tows, in the case of TBDCs), and (iii) the architecture of the reinforcing units within the composite; the latter is extremely complex in a TBDC material (as the tows are randomly oriented and randomly located), and extremely simple in a “Brick-and-Mortar” (BaM) composite (represented in Fig. 1a). Therefore, in order to explore the design space of TBDCs and identify potential routes to improve their tensile strength, we will first analyse the failure mechanisms of an equivalent BaM composite under longitudinal tension.

Considering a BaM composite as shown in Fig. 1a, where the bricks

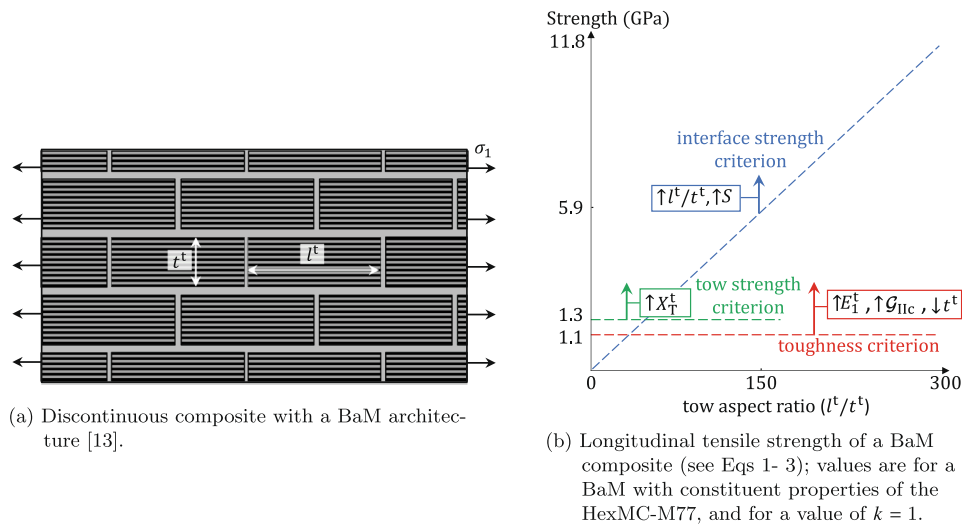


Fig. 1. Model material systems used to represent TBDCs. (For interpretation of the references to colour in this figure legend, the reader is referred to the web version of this article.)

are tows (with thickness t^t and length l^t) and the mortar is the tow-to-tow interface (with negligible thickness), its ultimate longitudinal tensile strength is bounded by the following criteria [13]:

- Tow strength criterion: for high aspect-ratio (length divided by thickness) tows, the longitudinal stresses at the centre of the tow transferred via shear of the interface may exceed the longitudinal tensile strength of the tow X_T^t . In this case, failure of the composite is governed by tensile fracture of the tows (i.e. fibre failure), at the overall composite stress

$$X_D^\infty = \frac{X_T^t}{k} \quad (1)$$

where k is the stress concentration factor due to the presence of tow end. For a perfectly staggered BaM composite, as shown in Fig. 1a, $k = 2$ and for a real TBDC with randomly located tow ends k is between 1 and 2 [21].

- Interface strength criterion: for low aspect-ratio tows, yielding of the interface limits the stress transfer to the tows [32], in a process that eventually leads to pull-out. Therefore, the overall composite strength, is limited by the interface shear strength (S), where the former is given by

$$X_D^\infty = \frac{l^t \cdot S}{2 \cdot t^t} \quad (2)$$

- Interface toughness criterion: for tows with high thickness, the strength of the discontinuous composite is bounded by a process governed by fracture mechanics, in which a mode-II crack propagates along the interface between tows [13], eventually also leading to pull-out of the tows. The strength of the composite, from a toughness-based formulation, is related to the interface mode-II fracture toughness \mathcal{G}_{IIc}^m , to the tow longitudinal Young's modulus E_1^t , and to the absolute value of tow thickness t^t by

$$X_D^\infty = \sqrt{\frac{2E_1^t \mathcal{G}_{IIc}^m}{t^t}} \quad (3)$$

It is important to notice that, while in Eq. 2 the strength is governed by the aspect-ratio (l^t/t^t) of the tows, this is not the case for Eq. 3, which is governed by the absolute value of the tow thickness t^t .

These three failure criteria act as boundaries of the ultimate

strength of BaM composites, and define the design space shown in Fig. 1b. The failure mechanisms mentioned above also dominate the tensile strength of TBDCs [5], and models based on BaM composites have been successfully used to model the response of TBDCs [21]. Therefore, the design space shown in Fig. 1b can be used to identify the qualitative effect of microstructural parameters on the tensile strength of TBDCs.

Considering the typical constituents (carbon-fibres and epoxy matrix) and tow dimensions (above 20 mm long and 0.1 mm thick) of TBDCs [2,11,10,3], the boundary governed by the interface toughness criteria (Eq. 3) is typically the most limiting one to the strength of TBDCs (Fig. 1b). This interface toughness boundary can be shifted to higher values of strength (closer to the boundary of the tow strength criterion) by using thinner tows with stiffer fibres, which will improve the tensile strength of a TBDC material. The remainder of this paper will focus on exploring and demonstrating the effectiveness of this concept.

2.2. Improving the strength of TBDCs via microstructure design

A physically-based model previously developed in the literature [21] to predict the strength of TBDCs will be here used to quantify the benefits of using thin tows of high-stiffness carbon fibres as the basic reinforcement of a TBDC material system. The key aspects of the model are here summarised:

- The random discontinuous material is locally idealised as an isotropic *equivalent laminate* (see Fig. 2a), with each lamina being a unidirectional discontinuous ply (with stiffness and strength properties given by those of a discontinuous material system, with the same tow geometry as in the randomly-oriented TBDC [21]); a constant number of discontinuous plies is assumed, oriented at equally-spaced angles, forming an isotropic layup.
- A multiscale model is used to predict the mechanical properties of the equivalent laminate. The longitudinal modulus of a UD discontinuous ply is calculated based on a shear-lag model [33]; the remaining elastic constants are obtained using the Halpin-Tsai equations [34] (assuming a transverse isotropic behaviour for the tows). Classical laminate theory (CLT) is then used to homogenise the elastic properties of the equivalent laminate.
- An Interactive Tension-Shear (ITS) criterion is used to predict the failure of a UD discontinuous ply under an in-plane stress state $\sigma = [\sigma_1, \sigma_2, \tau_{12}]$. It considers that failure of a UD discontinuous ply

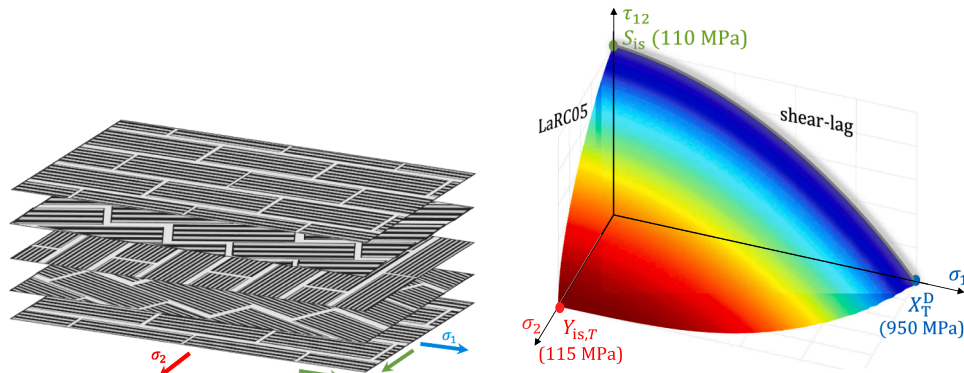


Fig. 2. Governing failure criteria for discontinuous composites. (For interpretation of the references to colour in this figure legend, the reader is referred to the web version of this article.)

can occur due to a combination of three failure mechanisms: (i) tow fracture, due to longitudinal tensile stresses σ_1 ; (ii) shear failure of the interface between neighbouring tows, which may occur due to progressive yielding (as in the interface strength criterion in Fig. 1b) or sudden debonding (as in the interface toughness criterion in Fig. 1b), resulting from the interaction between σ_1 , σ_2 , and τ_{12} ; and (iii) transverse tow/interfacial failure, due to σ_2 and τ_{12} . For the later, the matrix dominated failure criteria from the LaRC05 [35] is used, which includes the in situ effect on the transverse tensile and shear strengths of the UD plies. The combination of these failure modes leads to the definition of the failure surface shown in Fig. 2b, from which a failure index F_1 can be calculated for a discontinuous ply; the failure of a UD discontinuous ply occurs when the correspondent failure index $F_1(\sigma_1, \sigma_2, \tau_{12}) = 1$.

iv) The failure of the equivalent laminate is assumed to be governed by a first-ply-failure criterion [21], where the equivalent laminate fails as soon as the first ply fails.

It should be noted that this modelling approach neglects the intrinsic variability of TBDCs and therefore the predicted strength values are closer to those of a discontinuous equivalent laminate than to a randomly oriented TBDC [21]. Nevertheless, the results of this model can still be used to identify the trends of the influence of micro-mechanical properties on the overall strength of randomly-oriented TBDCs.

Table 1

Tow properties used as model inputs for the TBDC baseline configuration (HexMC-M77). Modulus values are in GPa, strength values are in MPa, toughness values are in kJ/m² and volume fraction in %. The values of Y_T and S are correspond to the raw strength values, which are corrected for in situ effects in $Y_{is,T}$ and S_{is} .

Material	E_1^t	E_2	G_{12}	ν_{12}	X_T^t	Y_T	Y_C	S	\mathcal{G}_{int}^{1c}	V^f
HexPly-M77 [43]	129 [†]	9.0 [‡]	5.6 [‡]	0.34 [‡]	1258 [†]	73 [‡]	200 [‡]	78	0.8 [‡]	57

[‡] Estimated values based on the literature [44].

[†] Values taken from uni-axial tensile tests on HexPly-M77 with $V_{HexPly-M77}^f = 51.3$ %, linearly scaled up to the nominal fibre content of the HexMC-M77 material ($V^f = 57$ %).

The envelope of the ITS for a UD discontinuous equivalent ply defined by the interaction between the in-plane longitudinal tension and shear stresses (σ_1 vs. τ_{12} , with $\sigma_2 = 0$, see Fig. 2b) is governed by the shear-lag stress transfer mechanism. Fig. 3a and b show how this failure envelope is influenced by t^t and E_1^t respectively, using as baseline the microstructure properties of a commercial TBDC system, the HexMC-M77 [10] (specified in Tables 1 and 2). For stiffer and thinner tows, a significant shift of the failure envelope to higher values of σ_1 is predicted. This effect reflects the more efficient stress transfer that occurs through shear-lag, delaying the onset of a mode-II crack propagating along the tow's interface and ultimately leading to failure. This allows for a

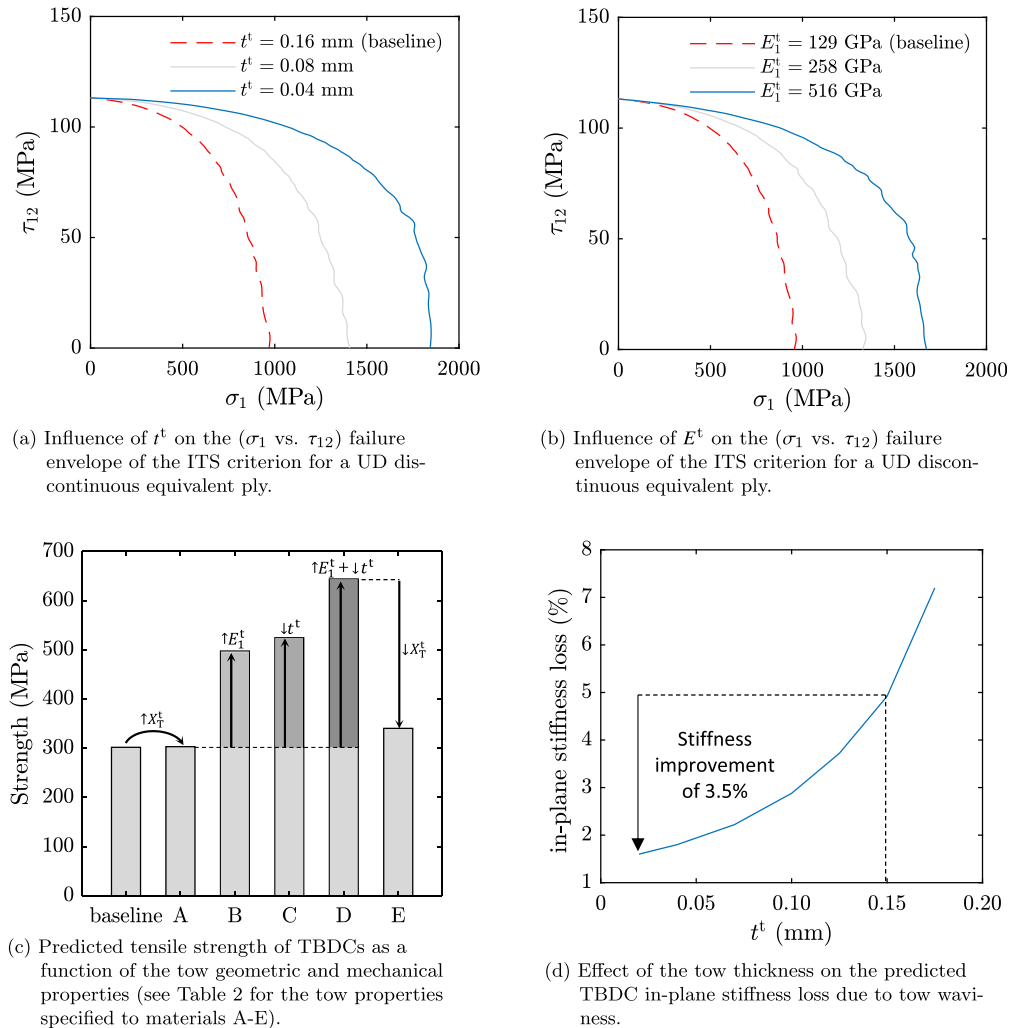


Fig. 3. Analysis of the influence of the different microstructural features/properties on the mechanical properties of TBDCs. The baseline material system is the HexMC-M77 [10], as defined in Tables 1 and 2.

Table 2

Properties used in the analysis of the influence of the tow mechanical properties on the strength of TBDCs.

Configuration	X_T^t (MPa)	t^t (μm)	E_1^t (GPa)
HexMC M77 - baseline	1258	0.164	129
A	2650	0.164	129
B	2650	0.164	516
C	2650	0.041	129
D	2650	0.041	516
E	1258	0.041	516

further exploitation of the mechanical properties of the fibres, maximising the mechanical properties of the TBDC.

The physically-based model is here used to explore the trends of the effect of the tow properties (tow strength X_T^t , stiffness E_1^t and thickness t^t) on the tensile strength of TBDCs. Table 1 summarises all the material inputs required for the model, and Table 2 presents several configurations with different tow properties analysed. The predicted TBDC strength for each configuration is presented in Fig. 3c, where the following trends can be identified:

- For configuration A, the increase in X_T^t over the baseline material does not lead to an increase in the TBDC strength, indicating that, for the baseline configuration, failure is governed by tow pull-out.
- For configurations B and C, the increase in the tow stiffness and the reduction of tow thickness (respectively) over configuration A lead to very significant increases in the TBDC strength. This is due to the shift to higher stress values of the toughness criterion boundary (see Fig. 1b), as result of a more efficient stress transfer mechanism (governed by shear-lag, see Eq. 3), enabling a better exploitation of the tow tensile properties.
- Configuration D is the one that presents the highest predicted TBDC strength, as it combines the benefits of both stiffer and thinner tows over configuration A. However, the increase of the TBDC strength for this configuration D is not given by a linear combination of those in configurations B and C.
- Configuration E combines the benefit of thin and stiff tows as in configuration D, but with a lower tensile strength X_T^t . The TBDC strength predicted for configuration E is significantly lower than that of configuration D (and only slightly higher than of the baseline), which indicates that the predominant failure mechanism in configurations D and E, is no longer tow pull-out but tow fracture instead; the strength of the TBDC in configuration E is therefore bounded by the low value of X_T^t .

The use of thinner tows has also been demonstrated to have a positive effect on the TBDC's in-plane modulus [36], by reducing the probability of tows with significant out-of-plane orientations. This is due to the more regular and "layered" microstructure that results from these configurations, which leads to a lower impact of the tow waviness on the in-plane modulus of the TBDC material, as shown in Fig. 3d.

3. Materials and experimental methods

3.1. Materials and manufacturing procedure

In order to demonstrate the potential improvements in the mechanical properties of TBDCs identified with the numerical models in Section 2, TBDC plates were manufactured using tows of high-modulus carbon-fibres spread into ultra-thin tapes and epoxy films, as described next. The spread tapes were produced by TeXtreme® spread tow technology (a state-of-the-art procedure for spreading tows into thin flat tapes with desired thickness and width) at Oxeon AB, using HS40 (High Modulus, HM) PAN-based and K13916 (Ultra High Modulus, UHM) pitch-based carbon-fibres. The nominal mechanical properties of the

Table 3

Mechanical properties of the different fibre types used in the experiments.

Fibre type	E^f (GPa)	X^f (MPa)	ϵ_{fail}^f (%)	Ref.
HS40 (HM)	425	4640	1.01	[41]
K13916 (UHM)	760	3000	0.40	[41]

fibres (modulus E^f , strength X^f and strain to failure ϵ_{fail}^f) are presented in Table 3. The spread tapes had a width of 20 mm, and an areal weight of 21 gsm (corresponding to a thickness of approximately 20 μm) or 105 gsm (corresponding to a thickness of approximately 100 μm) for the HM fibres, and of 105 gsm for the UHM fibres; the spread tapes were cut in 50 mm long pieces, hereby referred to solely as tapes. The epoxy resin used was supplied by Oxeon AB in the form of thin resin films, with an areal weight of 30gsm.

The tapes were manually placed at random locations and orientations on resin films, forming one equivalent lamina (EL), as schematically represented in Fig. 4a. In each EL (consisting in one resin film and 100 tapes) overlaps between the tapes were allowed, and the randomness of the tape positions and orientations was not constrained consciously. After the tape placement, heated de-bulks were performed on each EL; this consists in placing each EL in a vacuum bag on a heated RIFT table (at 70 °C) for 10 min, in order to ensure a better resin infusion. The final TBDC plate was obtained by stacking several ELs (in order to produce plates with the number of tapes specified in Table 4), as shown in Fig. 4b. During this stacking process, the reference direction of each EL was incrementally rotated by 90° in the stack, in order to further improve the randomness of tape orientations and the in-plane isotropy of the material. This stacking process was followed by a final heated de-bulk of the plate (ensuring a more uniform distribution of the resin along the through-the-thickness direction) before final curing; the plates were cured in an autoclave (with frayed edges and a caul plate) at 6 bars and 120°C for 1 h, after an initial 30 min stage of at 75 °C. Despite the use of the caul plate, some thickness and volume fraction variations occurred along the specimens, as shown in Table 4, due to the uneven number of tows along the thickness. Moreover, squeeze flow during the curing process was not monitored.

Five different plate configurations (described in Table 4 under IDs coded as <fibre type> - <nominal tape thickness> - <number of tapes in plate> - <testing direction>) were manufactured and tested in order to independently assess different effects:

- In-plane isotropy (HM-20-800-0 and HM-20-800-90): both plates were manufactured with the same specifications, although the specimens of each plate were tested at different orientations (0° and 90°) to the reference plate direction.
- Effect of the areal tape coverage (HM-20-800 and HM-20-1600): both plates were manufactured with the same fibre type and tape thickness, but with different total number of tapes in the plate ($N_{\text{tapes}} = 800$ and $N_{\text{tapes}} = 1600$, respectively).
- Effect of the tape thickness (HM-20-800 and HM-100-800): both plates were manufactured with the same fibre type and number of tapes, but with different tape thicknesses (20 and 100 μm).
- Effect of the fibre stiffness (HM-100-800 and UHM-100-800): both plates were manufactured with the same tape thickness and number of tapes, but with different fibre types (HM and UHM).

3.2. Testing and analysis

Each plate was cut into 5 rectangular specimens, 250 × 50 mm in length and width respectively, which were then subjected to a standard uni-axial tensile test, with a gauge length of 150 mm (following the ASTM-D3039 standard [37], and with a head displacement of 1 mm/min). The strain in the specimens was measured with an optical strain gauge [38]; the total strain was taken as the average strain measured by

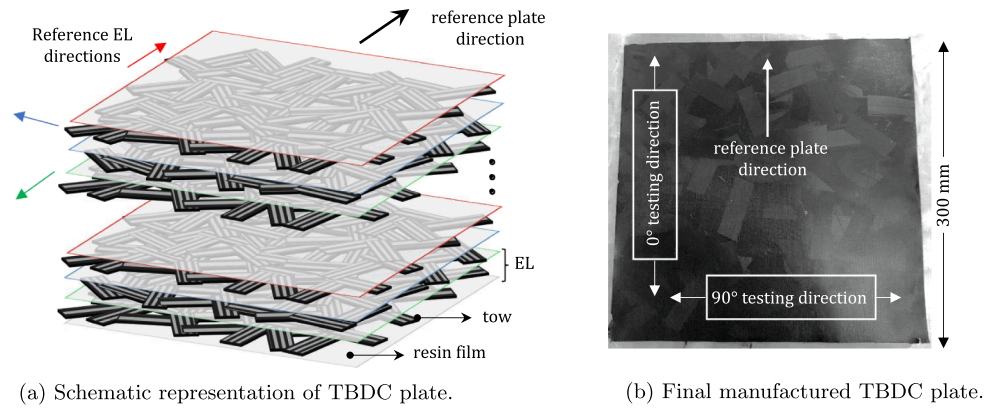


Fig. 4. Manufacturing procedure of the TBDC plates.

three virtual extensometers, each with a strain gauge length of 75 mm, evenly spaced along the specimen's width. Furthermore, the modulus of each specimen was taken as the (best fit) slope of the measured stress-strain curve between 0.05% and 0.2% strain. Emery cloth was used between the specimens and the testing grips, and the majority of tested specimens failed within the gauge section.

Optical micrographs were used to analyse the resulting microstructure of each plate configuration at three distinct cross-sections; the volume fraction of each cross-section was obtained from processing these three micrographs ($[0.15 \times 0.40]$ mm) using simple threshold algorithms. Images of the fracture surface of each specimen were taken using a standard camera, in order to identify the predominant failure mechanism in each plate configuration.

4. Results

4.1. Tensile test results

The results of the tensile tests are shown in Fig. 5; for all materials tested, the response was linear-elastic up to failure. All modulus and strength results presented in this section have been linearly scaled to a $V^f = 57\%$ (which is a typical value for commercial available TBDCs [10]), in order to allow for a direct comparison between different material systems. Fig. 5a shows the measured stiffness of the specimens from each plate configuration. The modulus values of the plates made with the HM fibres is relatively constant across the different plate configurations; this suggests that the fibre volume fraction measurements shown in Table 4 are representative of the plates manufactured, and that the linear scaling to $V^f = 57\%$ is appropriate. The plate with the UHM fibres yielded the highest average stiffness value, as expected, although with a large standard deviation.

Fig. 5b presents the both the average strength value measured for each plate configuration as well as the standard deviation:

- The highest tensile strength value of 600 MPa was achieved with the thin HS40 tapes, and in particular for the plate configuration with

1600 tapes.

- The strength difference between the HM-20-1600 plate and the HM-20-800 is quite significant, with a p -value = 0.06 (all p -values in this paper refer to two-sample (unequal variance) two-tailed t-test); since these two plates only differ in the total number of tapes, this difference can be explained by a more even areal tape coverage along the thickness of the specimen in the HM-20-1600 plate configuration. This leads to a lower probability of finding regions with a small number of tapes along the thickness direction (which trigger premature failure). This reflects the difficulty of achieving a good fibre areal coverage in a randomly oriented TBDC with a low ratio between the plate and the tape thicknesses.
- The HM-100-800 plate, with the thicker tape configuration, presents a significantly lower average strength value when compared to the thinner tape configurations (HM-20-800), with a p -value = 0.05. This is due to a more efficient stress transfer in the latter, and to an increase in the TBDC strength-bound dominated by the interface toughness (Eq. 3).
- The UHM-100-800 plate was the one that presented the lowest average strength; this is due to the combination of thick tapes, low fibre strength, and a lower total number of tapes. This was also the configuration with the most significant variability in the measured results, likely due to the fact that only 3 (out of 5) if the specimens produced valid failures (and only those 3 are included in Fig. 5b–d).

Fig. 5c shows the failure strain of the TBDCs (ϵ_{fail}^{TBDC}) tested; once again the HM-20-1600 configuration was the one that presented the highest ϵ_{fail}^{TBDC} , and the UHM-100-800 configuration presented the lowest value. However, by analysing the ratio between the TBDC failure strain and the fibre failure strain ($\epsilon_{fail}^{TBDC} / \epsilon_{fail}^f$), as done in Fig. 5d, one can better quantify the exploitation of the fibre strength within the TBDC, for each plate configuration: this suggests that the configuration with the UHM fibres (UHM-100-800) achieved a better exploitation of the fibre strength than the corresponding configuration with HM fibres (p -value = 0.17), due to a more efficient stress transfer mechanism promoted by the stiffer fibres in the former. However, the lower fibre strength of the UHM fibres (3000 MPa) compared to the HM fibres

Table 4
Configurations of the different TBDC plates manufactured.

Plate ID	Fibre type	Nominal t^l (μm)	Nominal N_{tapes}	Measured thickness (mm)	Measured V^f (%)	Testing direction* ($^\circ$)
HM-20-800-0	HS40	20	800	0.187 ± 0.021	47 ± 3.7	0
HM-20-800-90	HS40	20	800	0.194 ± 0.029	46 ± 3.5	90
HM-20-1600	HS40	20	1600	0.480 ± 0.040	46 ± 1.7	0
HM-100-800	HS40	100	800	0.902 ± 0.064	54 ± 3.2	0
UHM-100-800	K13916	100	800	0.715 ± 0.075	55 ± 5.0	0

* Testing direction of the specimens relative to the reference plate direction.

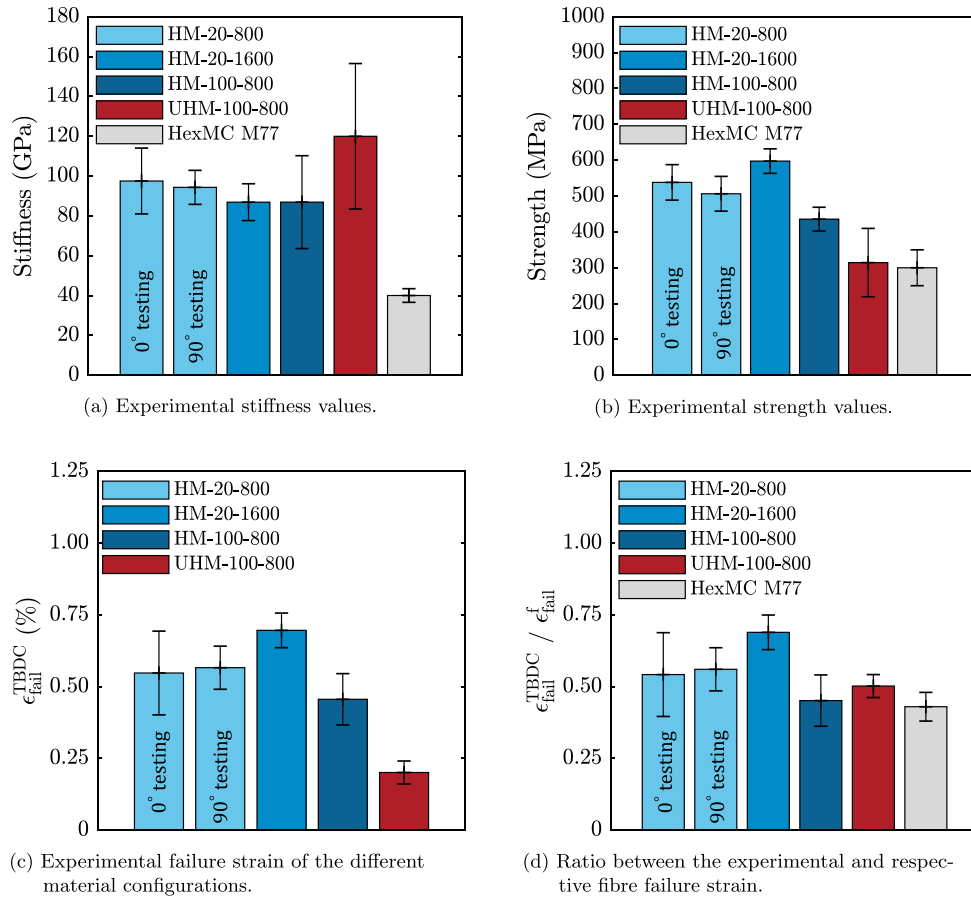


Fig. 5. Experimental tensile test results of the different TBDC configurations tested (scaled to $V^f = 57\%$), and comparison against the commercially available HexMC-M77 [10]; the error bars represent one standard deviation. (For interpretation of the references to colour in this figure legend, the reader is referred to the web version of this article.)

(4640 MPa) is limiting the TBDC strength value of the UHM material.

As previously mentioned in Section 3.1 and Table 4, HM-20-800 specimens were tested both at 0° and 90° testing directions, in order to verify whether in-plane isotropy was achieved. Fig. 5 shows that the properties measured at the two testing directions are identical, which supports the conclusion that the manufacturing process described in Section 3.1 indeed resulted in in-plane isotropy.

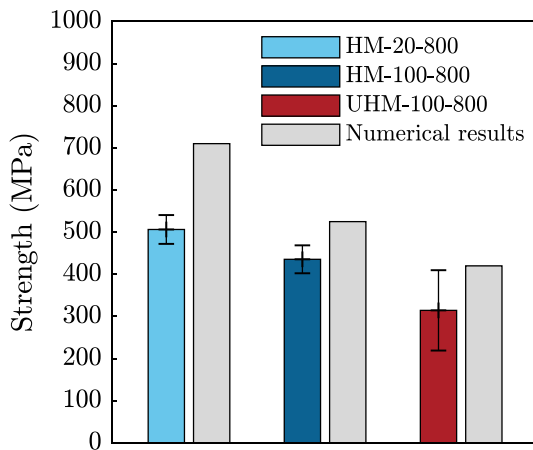


Fig. 6. Comparison between the numerical predictions and experimental results for the strength of three different plate configurations. (For interpretation of the references to colour in this figure legend, the reader is referred to the web version of this article.)

Fig. 6 compares the strength predicted by the model presented in Section 2 with the experimental results of three different plate configurations (HM-20-800, HM-100-800 and UHM-100-800). The numerical inputs for the model can be found in Table 3, except for the tape thickness t^f – which is shown in Table 4 for each plate configuration – and for the fibre-dominated tensile properties of the tows – which were taken as $E_1^t = E^f \cdot V^f$ and $X_1^t = X^f \cdot V^f$, with E^f and X^f as presented in Table 3. The analytical model captures the measured effect of the tape thickness and fibre stiffness on the strength of TBDCs, but predicts higher strength values when compared to those measured experimentally, for all cases. This is due to the intrinsic variability of the TBDC material system (where local weak spots govern failure of the material), which is not directly incorporated in the analytical model (as it considers quasi-isotropic equivalent laminates, see Fig. 2a). However, the relative magnitude of the influence of the different tape properties in the predicted TBDC strength are in good agreement with the experimental results.

4.2. Fracture surfaces

The fracture surfaces of a representative specimen taken from each plate configuration are shown Fig. 7. The fracture surfaces for the thin tape configurations (Fig. 7a and b) show no evidence of tape pull-out, and a clear evidence of tape fracture. For the thicker tape configurations (Figs. 7c and d), a mixture of tape pull-out and tape fracture was observed, reflecting the less efficient stress transfer that occurs for thicker tape configurations. The fracture surfaces of the thin tape configurations are remarkably different from those of the thick tapes, and reflect the predictions from the design stage drawn in Section 2.

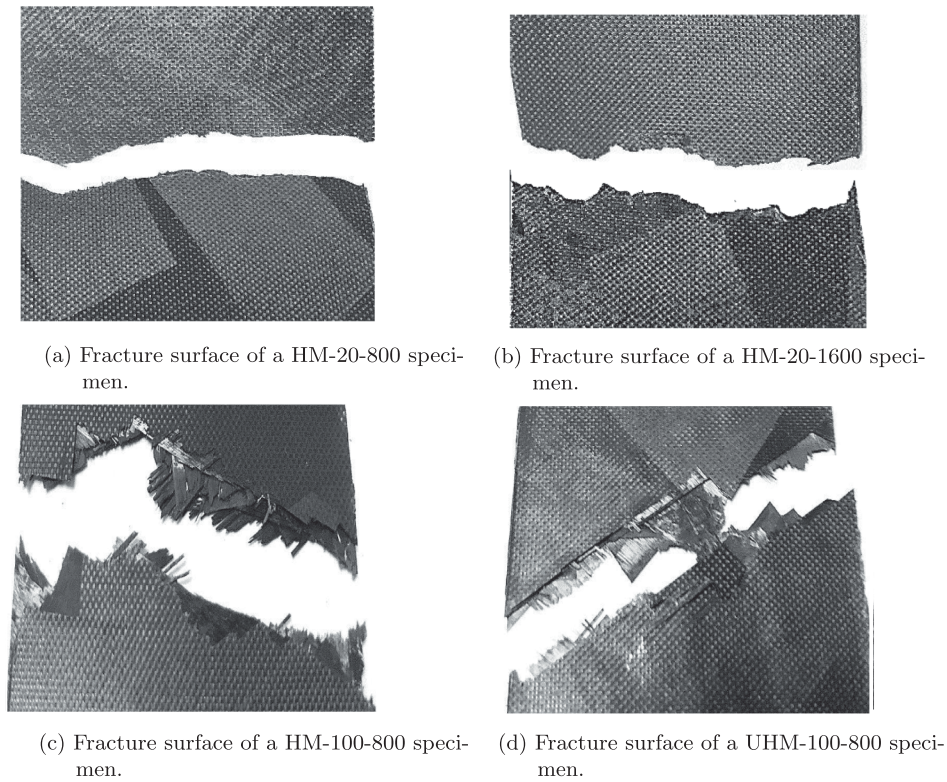


Fig. 7. Fracture surfaces of specimens from the different plate configurations.

4.3. Comparison with other material systems

Fig. 8 compares micrographs of four different materials systems: Fig. 8a and b are cross-sections of two commercially available TBDC materials systems [10,39]; the microstructures of these materials are very irregular, with the carbon fibre tows presenting significant through-the-thickness waviness and large resin rich regions. Fig. 8c corresponds to a cross-section of a conventional continuous-fibre composite [40], with its conventional regular and well structured microstructure. Finally, Fig. 8d and e show two different cross-sections of a HM-20-1600 specimen developed in this paper (these two were taken from two different cross sections a specimen); the microstructure of this material system presents a very little amount of tape waviness, and is visually more similar to the microstructure of the quasi-isotropic material system in Fig. 8c, than to the commercially available TBDCs in Fig. 8a and b.

The mechanical properties of the HM-20-1600 and UHM-100-800 configurations (which are the material systems that performed the best from the ones tested in this work) are compared to other carbon-fibre based material systems specified in Table 5; these include TBDC systems presented in the literature [4,29,30], the HexMC[®]-M77 [10] and the AMC[®] 8593 [11] commercially available TBDC material systems, and a widely-used aerospace-grade CF/epoxy continuous Quasi-Isotropic (QI) laminate. Fig. 9a shows that the HM-20-1600 and UHM-100-800 materials system have significantly higher average stiffnesses when compared to all other TBDC material systems. In Fig. 9c the HM-20-1600 material system turned out to be the one that presents the highest average strength of all TBDC-type materials.

Fig. 9b and 9d show how the ratio between the stiffness or strength of the TBDC and that of the fibre (E^{TBDC}/E^f and X^{TBDC}/X^f) differs for all material system. These results clearly show that the proposed HM-20-1600 configuration is the one that best exploits the fibre properties, due to enhanced stress transfer mechanism enabled by the ultra-thin and stiff tapes.

The mechanical properties of the UHM-100-800 and HM-20-1600

configurations are compared to those of a widely-used aerospace-graded quasi-isotropic laminate of continuous fibres (AS4 8552 [31]) in Fig. 10. Remarkably, the strength of HM-20-1600 (with a fibre tensile strength of 4640 MPa [41]) discontinuous material is practically the same as the one of the continuous fibre laminate (with a similar fibre tensile strength of 4619 MPa [42]). Moreover, due to the high modulus fibres used in both discontinuous configurations HM-20-1600 and UHM-100-800, the measured stiffness values are much higher than that of the AS4/8552 continuous fibre laminate.

5. Discussion

5.1. Effect of microstructure on mechanical properties

This work shows that, using ultra-thin tapes, TBDCs with a more regular microstructure are achieved (compared to conventional TBDCs with conventional thickness tows), as shown in Fig. 8d. This leads to improvements in stiffness (as previously suggested in the literature [3–5], and corroborated by the slightly higher Young's modulus of the HM-20-800 material compared to the HM-100-800 in Fig. 5a), as the tapes present less out-of-plane orientations, and hence lower reductions of in-plane stiffness due to tow/tape waviness [36]. For instance, Fig. 3d suggests that using 20 μm tapes rather than 150 μm tows should lead to a 3.5 % improvement in the in-plane stiffness of a TBDC.

Furthermore, this more regular microstructure is also less prone to weak spots within the material (such as resin pockets) which generally trigger premature failure, and hence also contributes to the significant increase in the ultimate strength of the material (compare HM-20-800 with HM-100-800 in Fig. 5b). In addition to the effect on the material's microstructure, the use of thin and stiff tapes also leads a more efficient stress transfer between the tapes, as it has been explained by the shear-lag models discussed in Section 2 (Eq. 3), and hence to a better exploitation of the mechanical properties of the fibres, as shown by the HM-20-1600 and UHM-100-800 configurations in Fig. 5d.

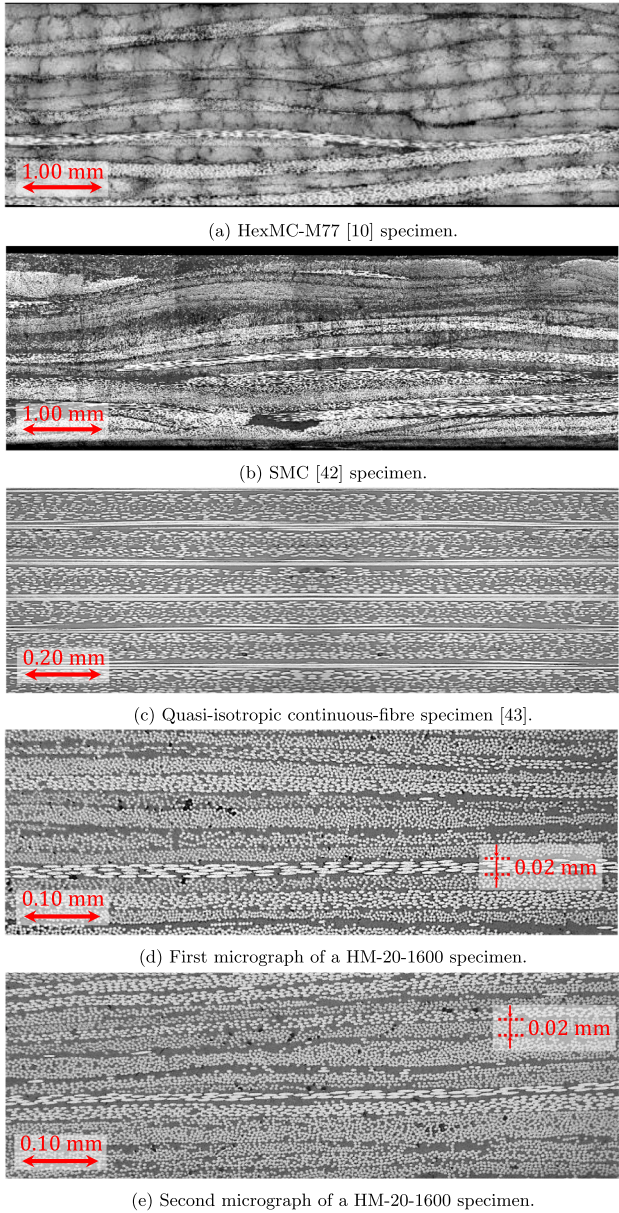


Fig. 8. Micrographs of cross-sections of different material systems.

5.2. Improvement over existing materials

5.2.1. Benchmark against other TBDCs

The stiffness improvements achieved with the ultra-thin and stiff tape based TBDCs shown in Fig. 9a are essentially due to the higher stiffness of the HM and UHM fibres (see Table 3), compared to standard modulus fibres. However, there is a small difference between the

stiffness of the HM-20-800 and HM-100-800 plate configurations, with the later presenting lower stiffness values (see Fig. 5a). This may be due to the more wavy disposition of the thicker tapes in comparison to the thinner tapes, leading to higher stiffness knock-downs [36], which is in agreement with the numerical predictions shown in Fig. 3d.

The average strength value of 600 MPa, obtained with the HM-20-1600 plate configuration (see Fig. 5b), represents an increase of 100% when compared to the strength of the commercially available materials and of $\approx 20\%$ when compared to the UT-CTT materials [4], which were the TBDC system with the highest strength previously reported in the literature. The enhancement of the stress-transfer mechanisms enabled by the use of ultra-thin and stiff tapes delays the on-set of tow pull-out (governed by toughness criterion, see Eq. 3) and promotes failure by tape fracture, as evidenced by the fracture surfaces of Fig. 7a and b.

Although the tape-based composites proposed in this paper have been only tested under tensile loading, the shear and compressive properties (stiffness and strength) are also expected to be higher than in conventional TBDCs, again due to the use of stiffer fibres and to the enhanced stress-transfer mechanism facilitated by the ultra-thin tapes. Moreover, compressive properties are expected to benefit even more from the more regular microstructure, with less pronounced out of plane orientations of the tapes, which will delay the onset of tow debonding and fibre kinking.

5.2.2. Benchmark against continuous-fibre composites

The comparison between the mechanical properties of the best proposed configurations (HM-20-1600 and UHM-100-800) against those of a continuous QI laminate in Fig. 10, shows that it is possible to match the strength of a continuous fibre laminate and surpass its stiffness using a composite with a discontinuous microstructure.

While the two fibre-types used in the discontinuous HM-20-1600 composite and in the continuous AS4/8552 (respectively HS40 [41] and AS4 [42] are different, they have very similar single-fibre tensile strengths (around 4600 MPa). Therefore, the discontinuous HM-20-1600 is able to reach nearly the same strength as the AS4/8552 continuous composite not due to an improved fibre strength, but to an improved stress-transfer within the tapes. This improved stress-transfer has been facilitated by optimising the two microstructural parameters identified in Section 2.1: (i) the thickness of the tapes/plies ($\approx 20 \mu\text{m}$ in the discontinuous composite, and $\approx 125 \mu\text{m}$ in the continuous composite), and (ii) the stiffness of the fibres (425 GPa in the discontinuous composite, and 231 GPa [42] in the continuous composite).

The higher stiffnesses measured for the discontinuous composites (HM-20-1600 and UHM-100-800) compared to the continuous-fibre laminate (AS4/8552) are a direct result of using stiffer fibres in the former: the Young's moduli of the HM and UHM fibres are 425 and 760 GPa respectively (Table 3), and the Young's modulus of the AS4 fibres is 231 GPa. Nevertheless, one should note that the UHM fibres pose significant manufacturability challenges when used in a continuous-fibre composite, and that these challenges are alleviated in a discontinuous-fibre composite, as will be further discussed in the next section.

Altogether, the results in Fig. 10 highlight the great potential that this new class of high-performance discontinuous composites offer, as

Table 5

Configurations of the different CFRP systems compared in Fig. 9.

Material ID	Material system description	V_f (%)	Ref.
DCFP	T700 carbon fibre/epoxy, manufactured with modified DCFP	45	[29]
HexMC-M77	Carbon epoxy material system for compression moulding	57	[10]
AMC8593	PAN-based carbon epoxy material system (moulding compound)	47	[11]
APC-2/AS4	Carbon/PEEK CYTEC APC-2/AS4 material system	61	[30]
UT-CTT	Ultra-thin (50 μm) carbon fibre/thermoplastic system	55	[4]
AS4 8552	Continuous fibre quasi-isotropic laminate	60	[31]
UHM-100-800	Thin (100 μm) and UHM carbon fibre/epoxy system	54	
HM-20-1600	Ultra-thin (20 μm) and HM carbon fibre/epoxy system	46	

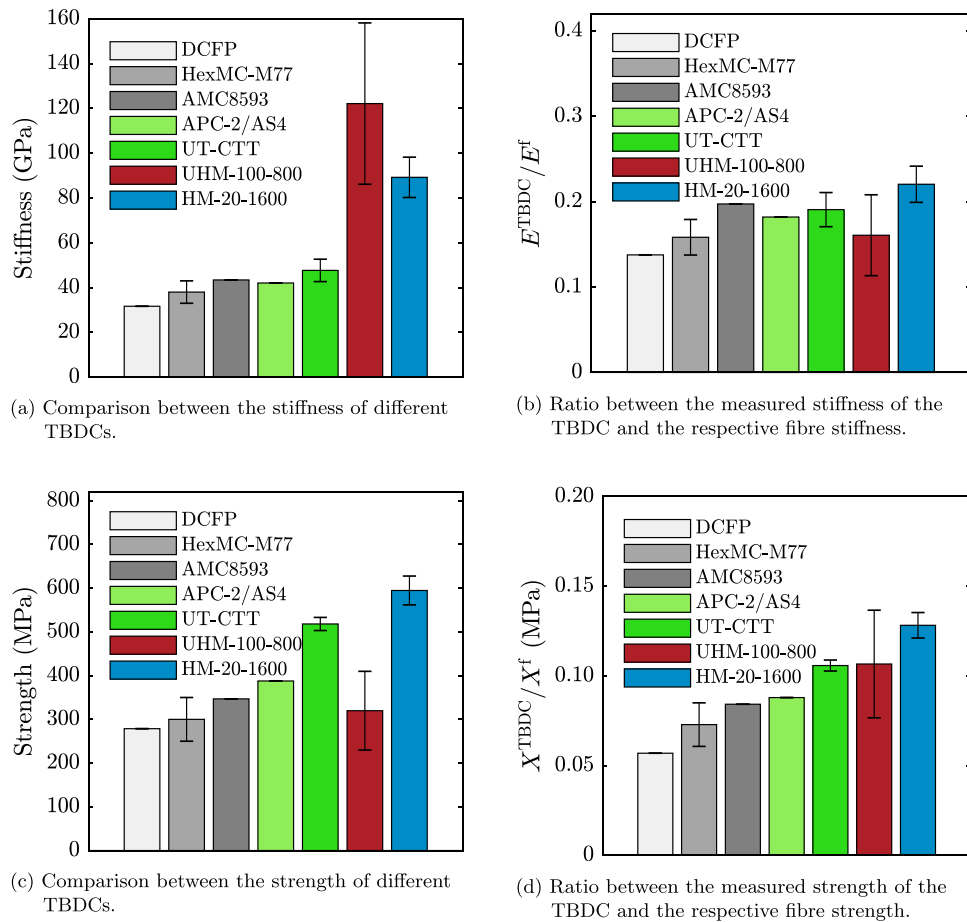


Fig. 9. Comparison of the mechanical properties between the HM-20-1600 material proposed in this study, and discontinuous material systems reported in the literature (specified in Table 5). The mechanical properties of all materials have been linearly normalised to $V^f = 57\%$ for comparison purposes. (For interpretation of the references to colour in this figure legend, the reader is referred to the web version of this article.)

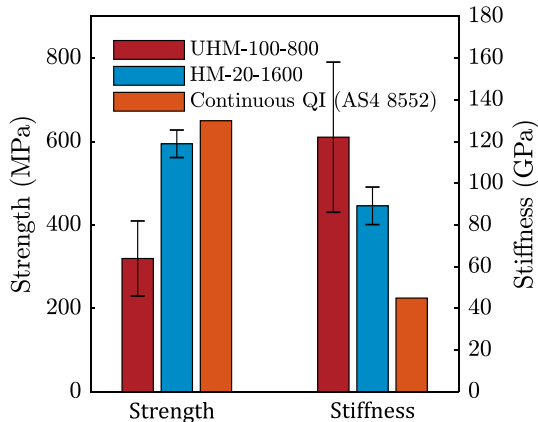


Fig. 10. Comparison between the mechanical properties of the HM-20-1600 and UHM-100-800 configurations and a continuous fibre QI laminate (specified in Table 5). (For interpretation of the references to colour in this figure legend, the reader is referred to the web version of this article.)

they are able to bridge the gap in mechanical properties that typically exists between continuous and discontinuous fibre composites, while still retaining the advantages of design flexibility and manufacturability of discontinuous composites, as discussed in the next section.

5.2.3. Design flexibility and manufacturability

It has been suggested in the literature [3,5] that the strength of TBDCs increases with plate thickness (for a constant tow thickness); this

is corroborated by the slightly higher strength and failure strain of the HM-20-1600 configuration when compared to the HM-20-800 configuration (see Fig. 5b–d). This effect can be explained by two factors: firstly, thicker specimens have a smaller fraction of tapes at the surface of the specimen, and these surface tapes cannot transfer stresses as effectively as those well-embedded in the through-the-thickness direction; secondly, thicker specimens have a larger average number of tapes in the through-the-thickness direction, which increases the homogeneity of mechanical properties in comparison with thinner specimens [36]. Consequently, there is a limitation for the minimum thickness that can be accepted in components manufactured with TBDC systems with conventional tow thicknesses. This limitation can be relaxed significantly through the use of ultra-thin tapes, as shown by the results in Figs. 5 and 9:

- Firstly, the mechanical properties of the plates manufactured with ultra-thin tapes were considerably higher than those of conventional TBDCs (see Figs. 5 and 9), even though the plate thickness of the former was below 0.5 mm.
- Secondly, the similar properties observed with the two HM-20-800 plates tested at different directions (see Fig. 5) suggest that using ultra-thin tapes to make TBDCs enables the manufacture of shell-type structures with wall thicknesses lower than 0.2 mm, with in-plane isotropy.

Consequently, TBDCs manufactured with ultra-thin tapes offer much more design flexibility than conventional TBDCs, and allow for production of shell-type structures with very thin walls (which is useful e.g. for body-in-white parts of cars).

Fig. 10 shows that TBDCs made of ultra-thin tapes of HM fibres combine (i) a similar strength and even higher stiffness than those of aerospace-graded composites with (ii) the improved manufacturability and design flexibility of a discontinuous and random microstructure. This concept has been proven in this work using a manual manufacturing method, but it could be realised at an industrial scale by creating SMC-type intermediate materials (similar to HexMC [10] and carbon-SMC [39]), but using ultra-thin (spread) tapes of (ultra-) high modulus fibres and fast-curing matrices; these intermediate materials could then be directly used in compression moulding, with several advantages over conventional continuous-fibre composites:

- Allowing for the production of parts within a matter of minutes and out-of-the-autoclave, and with minimal manual work;
- Allowing for the production of complex 3D geometries (rather than 2D shells) with local embedded reinforcements where they are needed most (rather than relying on ply-drops and bonded stiffeners, as often done with continuous-fibre composites).
- Possibility of using UHM fibres - which are extremely stiff but very brittle - to manufacture parts/components with complex geometries; this is enabled by the discontinuous architecture of TBDCs which allow the fibres to flow during the manufacturing process, and is not easily achievable with continuous-fibre architectures due to the combination of limited drapeability and fibre brittleness.
- Reducing significantly the amount of waste generated by material cut-offs.

6. Conclusions

This work has successfully proposed, designed and demonstrated a pathway to increase the stiffness and ultimate tensile strength of tow-based discontinuous composites. The main conclusions are summarised below:

- Quasi-isotropic TBDCs manufactured with ultra-thin (20 μm) and high-modulus (450 GPa) carbon-fibre tapes reached a tensile strength of 600 MPa and stiffness of 90 GPa. This represents a stiffness and strength increase of 100% when compared to commercially available TBDC materials, and of 20% when compared to the TBDC material system with the highest strength previously reported in the literature.
- This work demonstrates that TBDCs manufactured using ultra-thin and high-modulus carbon-fibre tapes can reach the tensile strength of conventional aerospace-grade QI laminated CFRP, and overcome their stiffness.
- The use of thin and stiff tapes in the manufacture of TBDCs leads to this significant improvement in mechanical properties by enhancing the stress transfer mechanisms within the material and suppressing matrix/interface dominated failure mechanisms. This allows for a better exploitation of the mechanical properties of the fibres, which has been demonstrated by the features of the fracture surfaces of these TBDCs, which were dominated by fibre-failure rather than by tape pull-out.
- Test results suggest that there is a reduction in tensile strength for specimens with a small ratio between the specimen thickness and tape thickness. This indicates that TBDCs with ultra-thin tapes can be used to manufacture components with very thin walls, removing several design barriers and offering more design flexibility over conventional TBDCs (based on tows with conventional thicknesses).

This work shows the potential of ultra-thin and stiff TBDCs as a high-performance and highly-manufacturable material, able to comply with the stiffness and strength requirements of primary structural applications and suitable for a wider range of part geometries and more automated manufacturing processes when compared to continuous-fibre composites. These materials can potentially change the way in

which composite materials are used in several industries (automotive, aerospace, sport and others), and at the same time open the use of high-performance composite materials to new industries with different manufacturability constraints.

CRedit authorship contribution statement

M. Alves: Conceptualization, Methodology, Investigation, Software, Formal analysis, Writing - original draft. **D. Carlstedt:** Conceptualization, Methodology, Writing - review & editing. **F. Ohlsson:** Writing - review & editing. **L.E. Asp:** Conceptualization, Methodology, Writing - review & editing, Supervision, Funding acquisition. **S. Pimenta:** Conceptualization, Methodology, Writing - review & editing, Supervision, Funding acquisition.

Declaration of Competing Interest

The authors declare that they have no known competing financial interests or personal relationships that could have appeared to influence the work reported in this paper.

Acknowledgements

The research leading to these results has been done within the framework of the FiBreMoD project and has received funding from the European Union's Horizon 2020 research and innovation programme under the Marie Skłodowska-Curie grant agreement No. 722626. S. Pimenta also acknowledges the support from the Royal Academy of Engineering in the scope of her Research Fellowship on 'Multiscale discontinuous composites for large scale and sustainable structural applications' (2015–2019). L. E. Asp acknowledges the support from VINNOVA via the LIGHTer Academy.

The authors also acknowledge S.K. Nothdurfter and K. Schuffenhauer (from the department of Advanced Composites and Lightweight Structures Development of Automobili Lamborghini S.p.A.) for several interesting discussions.

References

- [1] Harper LT. Discontinuous carbon fibre composites for automotive applications. University of Nottingham [Ph.D. thesis], 2006.
- [2] Selezneva M, Lessard L. Characterization of mechanical properties of randomly oriented strand thermoplastic composites. *J Compos Mater* 2016;50(20):2833–51.
- [3] Feraboli P, Peitso E, Deleo F, Cleveland T, Stickler PB. Characterization of prepreg-based discontinuous carbon fiber/epoxy systems. *J Reinf Plast Compos* 2009;28(10):1191–214.
- [4] Wan Y, Takahashi J. Tensile properties and aspect ratio simulation of transversely isotropic discontinuous carbon fiber reinforced thermoplastics. *Compos Sci Technol* 2016;137:167–76.
- [5] Li Y, Pimenta S, Singgih J, Nothdurfter S, Schuffenhauer K. Experimental investigation of randomly-oriented tow-based discontinuous composites and their equivalent laminates. *Compos Part A: Appl Sci Manuf* 2017;102:64–75.
- [6] Darvell M. Randomized CFRTT tape piece laminates in structural automotive applications. KTH Royal Institute of Technology [MSc Thesis], 2015.
- [7] Visweswaraiyah SB, Selezneva M, Lessard L, Hubert P. Mechanical characterisation and modelling of randomly oriented strand architecture and their hybrids – A general review. *J Reinf Plast Compos* 2018;37(8):548–80.
- [8] ASDNews. Nordam Pioneers Hexmc Composite Window Frames for Boeing 787 Dreamliner, 2007.
- [9] Roy S, Yousefpour A, Bednar F, Beaulieu P. Compression molding of composite tailboom frames. In: 70th American Helicopter Society International Annual Forum, vol. 3, Montreal, May 2014.
- [10] Hexcel. HexMC User Guide. https://www.hexcel.com/user_area/content_media/raw/HexMC_UserGuide.pdf, 2014. [Online; accessed 04-April-2019].
- [11] Composites Q. AMC8590 Technical Data Sheet. <https://www.quantumcomposites.com/pdf/datasheets/amc/Quantum-AMC-8590-20126-76-8.pdf>, 2014. [Online; accessed 08-April-2019].
- [12] Wan Y, Takahashi J. Tensile and compressive properties of chopped carbon fiber tapes reinforced thermoplastics with different fiber lengths and molding pressures. *Compos Part A: Appl Sci Manuf* 2016;87:271–81.
- [13] Pimenta S, Robinson P. An analytical shear-lag model for composites with 'brick-

- and-mortar' architecture considering non-linear matrix response and failure. *Compos Sci Technol* 2014;104:111–24.
- [14] Pimenta S, Ahuja A, Yong A. Damage tolerant tow-based discontinuous composites. In: ICCM20, Copenhagen, Denmark, July 2015.
- [15] Kravchenko SG, Sommer DE, Pipes RB. Uniaxial strength of a composite array of overlaid and aligned prepreg platelets. *Compos Part A: Appl Sci Manuf* 2018;109:31–47.
- [16] Dvorak GJ, Laws N. Analysis of progressive matrix cracking in composite laminates II. First ply failure. *J Compos Mater* 1987;21:309–29.
- [17] Camanho PP, Dávila CG, Pinho ST, Iannucci L, Robinson P. Prediction of in situ strengths and matrix cracking in composites under transverse tension and in-plane shear. *Compos Part A: Appl Sci Manuf* 2006;37:165–76.
- [18] Arteiro A, Catalanotti G, Reinoso J, Linde P, Camanho PP. Simulation of the mechanical response of thin-ply composites: From computational micro-mechanics to structural analysis. *Arch Comput Methods Eng* 2018.
- [19] Sih S, Kim RY, Kawabe K, Tsai SW. Experimental studies of thin-ply laminated composites. *Compos Sci Technol* 2007;67:996–1008.
- [20] Amacher R, Cugnoni J, Botsis J, Sorensen L, Smith W, Dransfeld C. Thin ply composites: Experimental characterization and modeling of size-effects. *Compos Sci Technol* 2014;101:121–32.
- [21] Li Y, Pimenta S. Development and assessment of modelling strategies to predict failure in tow-based discontinuous composites. *Compos Struct* 2019;209:1005–21.
- [22] Selezneva M, Roy S, Lessard L, Yousefpour A. Analytical model for prediction of strength and fracture paths characteristic to randomly oriented strand (ROS) composites. *Compos Part B: Eng* 2016;96:103–11.
- [23] Selezneva M, Roy S, Meldrum S, Lessard L, Yousefpour A. Modelling of mechanical properties of randomly oriented strand thermoplastic composites. *J Compos Mater* 2017;51(6):831–45.
- [24] Feraboli P, Cleveland T, Stickler P, Halpin J. Stochastic laminate analogy for simulating the variability in modulus of discontinuous composite materials. *Compos Part A: Appl Sci Manuf* 2010;41(4):557–70.
- [25] Chen Z, Huang T, Shao Y, Li Y, Xu H, Avery K, et al. Multiscale finite element modeling of sheet molding compound (smc) composite structure based on stochastic mesostructure reconstruction. *Compos Struct* 2018;188:25–38.
- [26] Harper L, Qian C, Luchoo R, Warrior N. 3D geometric modelling of discontinuous fibre composites using a force-directed algorithm. *J Compos Mater* 2016. 0021998316672722.
- [27] Taketa I, Matsutani H. Effect of fiber length on the tensile strength of uni-directionally arrayed chopped strands. *Adv Compos Mater* 2019:1–12.
- [28] Kravchenko SG, Sommer DE, Denos BR, Favaloro AJ, Tow CM, Avery WB, et al. Tensile properties of a stochastic prepreg platelet molded composite. *Compos Part A: Appl Sci Manuf* 2019;124. 105507.
- [29] Harper L, Burn D, Johnson M, Warrior N. Long discontinuous carbon fibre/polypropylene composites for high volume structural applications. *J Compos Mater* 2018;52(9):1155–70.
- [30] Selezneva M, Kouwonou K, Lessard L, Hubert P. Mechanical properties of randomly oriented strands thermoplastic composites. In: ICCM19, Montreal, Canada, July 2018.
- [31] Feraboli P, Peitso E, Deleo F, Cleveland T, Stickler PB. Characterization of prepreg-based discontinuous carbon fiber/epoxy systems. *J Reinf Plast Compos* 2009;28(10):1191–214.
- [32] Kelly A, Tyson W. Tensile properties of fibre-reinforced metals: Copper/tungsten and copper/molybdenum. *J Mech Phys Solids* 1965;13(6):329–50.
- [33] Henry J, Pimenta S. Semi-analytical simulation of aligned discontinuous composites. *Compos Sci Technol* 2017;144:230–44.
- [34] Affdl JCH, Kardos JL. The Halpin-Tsai equations: A review. *Polymer Eng Sci* 1976;16(5):344–52.
- [35] Pinho S, Darvizeh R, Robinson P, Schuecker C, Camanho P. Material and structural response of polymer-matrix fibre-reinforced composites. *J Compos Mater* 2012;46(19–20):2313–41.
- [36] Alves M, Pimenta S. The influence of 3d microstructural features on the elastic behaviour of tow-based discontinuous composites. *Compos Struct*, 2020 [in preparation].
- [37] ASTM International. Standard test method for tensile properties of polymer matrix composite materials. West Conshohocken; PA, 2002.
- [38] IMetrum. iMetrum LTD, Non Contact Precision Measurement. Simulia, 2018.
- [39] Mitsubishi Chemical Corporation. Pyrofil STR120 datasheet.
- [40] Mencattelli L, Pinho ST. Ultra-thin-ply cfrp bouligand bio-inspired structures with enhanced load-bearing capacity, delayed catastrophic failure and high energy dissipation capability. *Compos Part A: Appl Sci Manuf* 2019. 105655.
- [41] Mitsubishi Chemical Carbon Fiber and Composites. <http://mccfc.com>, 2019. [Online; accessed 03-October-2019].
- [42] Hexcel. HexTow AS4 Product Data Sheet. https://www.hexcel.com/user_area/content_media/raw/AS4_HexTow_DataSheet.pdf, 2019. [Online; accessed 03-February-2020].
- [43] Hexcel. HexPly M77 Product Data. <https://www.hexcel.com/Resources/DataSheets/Prepreg>, 2017. [Online; accessed 04-April-2019].
- [44] Kaddour A, Hinton M. Maturity of 3d failure criteria for fibre-reinforced composites: Comparison between theories and experiments: Part b of wwfe-ii. *J Compos Mater* 2013;47(6–7):925–66.